Nuclear Instruments and Methods in Physics Research A 652 (2011) 178–182

Contents lists available at ScienceDirect

Nuclear Instruments and Methods in Physics Research A

journal homepage: www.elsevier.com/locate/nima

Characterization of etch pit formation via the Everson-etching method on CdZnTe crystal surfaces from the bulk to the nanoscale

Lucile C. Teague [a,*], Martine C. Duff [a], James R. Cadieux [a], Raji Soundararajan [b], Charles R. Shick Jr.[a], Kelvin G. Lynn [b]

[a] Savannah River National Laboratory, Aiken, SC 29808, USA
[b] Center for Materials Research, Washington State University, Pullman, WA 99163, USA

ARTICLE INFO

Available online 29 September 2010

Keywords:
Etching
CZT
CdZnTe
AFM
Surface

ABSTRACT

A combination of atomic force microscopy, optical microscopy, and mass spectrometry was employed to study CdZnTe crystal surface and used etchant solution following exposure of the CdZnTe crystal to the Everson etch solution. We discuss the results of these studies in relationship to the initial surface preparation methods, the performance of the crystals as radiation spectrometers, the observed etch pit densities, and the chemical mechanism of surface etching. Our results show that the surface features that are exposed to etchants result from interactions with the chemical components of the etchants as well as pre-existing mechanical polishing.

1. Introduction

Over the last several years, it has been established that the presence of structural heterogeneities, such as twinning, pipes, grain boundaries (polycrystallinity), and "secondary" phases (SPs)[1–12] has an adverse impact on the performance of CdZnTe (CZT) semiconductor materials grown for use as room temperature gamma-ray and X-ray spectrometers. At present, researchers are investigating variations in crystal growth methods in order to reduce these structural heterogeneities and improve crystal quality. To determine the effectiveness of their modifications, crystal growers need reliable methods to assess defect density. To date, research and industrial groups have utilized a variety of surface etching techniques to examine the quality of CdZnTe crystals [13–18]. The Nakagawa etch (N-etch) [18] and the Everson etch (E-etch) [13] are the two different etchants utilized to analyze crystal quality. The location and density of etch pits (EPs) formed on the surface of CZT crystals etched using these methods have been attributed to the dislocation density and distribution of defects within the crystals because they are associated with exit points of dislocations within the crystal at the crystal surface [13,14].

Previous reports with E-etch and similar etchants have examined surface etching and EP formation on CZT and CdTe surfaces at the micron scale with optical and electron microscopy techniques such as SEM and TEM, and on CdTe/Si epilayers with atomic force microscopy (AFM) although the specific etching mechanisms are not known at the micro- and nanoscale [13–17,19]. In this study, we utilize a combination of high-resolution AFM and inductively coupled plasma mass spectrometry (ICP-MS) to gain a more thorough understanding of the significance of the surface features exposed (EPs) following these types of etches with respect to the bulk crystal properties and to gain further insight into the mechanisms by which the E-etch causes pitting on the CZT surface.

2. Experimental techniques

2.1. Crystal growth and surface preparation

Both the crystals used for this study are semi-insulating n-type, labeled CG54.AB.AD.1.D2 (10 mm × 10 mm × 1.89 mm) and CG54.AB.AD.1.E3 (3 mm × 7 mm × 1.9 mm) and are hereby referred to as D2 and E3, respectively. Each crystal was cut from the middle of a single crystal CdZnTe (10% Zn) ingot grown at the estimated stoichiometry of $Cd_{(1-x)}Zn_{(x)}Te$ using the electrodynamic gradient method (no mechanical movement of the furnace or the ampoule). All metals used during the growth process were of >6N purity. Feed materials were doped with indium (In) to compensate for electrical defects related to Cd loss that occurs during growth and the ingot was grown with an

Abbreviations: CZT, CdZnTe; AFM, atomic force microscopy; NIST, National Institute of Standards and Technology; SEM, scanning electron microscopy; TEM, transmission electron microscopy; ICP-MS, inductively coupled plasma mass spectrometry; SPs, secondary phases; EPs, etch pits; EtOH, ethanol; Br-MeOH, bromine methanol; E-etch, Everson etch; N-etch, Nakagawa etch

* Corresponding author. Tel.: +1 803 514 0226; fax: +1 803 725 4478.
E-mail address: lucile.teague@srnl.doe.gov (L.C. Teague).

0168-9002/$ - see front matter © 2010 Elsevier B.V. All rights reserved.
doi:10.1016/j.nima.2010.09.061

excess of 0.0375% by weight Te. Following cutting, the crystal was annealed at 75 °C in oxygen ($O_{2(g)}$) for 8 h.

A series of polishing steps with alumina (Al_2O_3) slurry (particle sizes of 9 μm down to 0.3 μm) was used to polish the CZT crystal surface. Ultrasonic cleaning was carried out at the end of every polishing step, and after the final polishing step the crystal was rinsed with ethanol (EtOH), wiped with a soft laboratory-wipe, and Au contacts were sputtered on the two largest opposing sides for detector measurements using the planar configuration. The performance of the crystal as a radiation spectrometer was measured for ^{57}Co, ^{241}Am, and ^{137}Cs. After performance measurements were taken, both crystals were then polished with 0.05 μm Al_2O_3 slurry in ~1% HCl solution in distilled water to remove the Au contacts. The surface of crystal D2 was additionally chemomechanically polished on a soft micro-cloth with ~2 mL of bromine (Br_2) in 100 mL methanol (MeOH) for about 5 min followed by a final MeOH rinse.

After polishing, each of the crystals were exposed to an E-etch solution [1:4:25, HF:HNO_3:lactic acid (85%)] for ~2 min. The crystal was removed from the etchant solution, rinsed several times with deionized H_2O ($\geq$ 18 MΩ cm), and was allowed to dry in the hood. The used etchant solution for sample E3 and a second reagent blank solution [1:4:25, HF:HNO_3:lactic acid (85%)] were set aside for further analysis by ICP-MS. The crystal surface was then gently wiped with EtOH.

2.2. Inductively coupled plasma-mass spectrometry analysis

For ICP-MS analysis, 2–3 mL of 8 M HNO_3 was added to the etchant and reagent blank solutions in Teflon beakers, and they were evaporated to near dryness on a hot plate. The acid addition and evaporation was repeated two more times and the subsequent residues were diluted to a 30 mL volume with 10% HNO_3. The solutions were transferred to acid-washed polypropylene sample vials and submitted for ICP-MS analysis.

Semi-quantitative ICP-MS was used to analyze the 30 mL of sample solution with a matrix of 10% HNO_3. Each sample was spiked with a 10 ppb In internal standard solution. The analysis of a NIST-traceable (National Institute of Standards and Technology), multi-element standard (10 ppb In and 50 ppb Li, Mg, Co, Ni, Sr, Cd, and Bi) was followed by the sequential analysis of: an initial calibration validation standard (10 ppb In, 10 ppb Rh, and 25 ppb Li, Mg, Co, Ni, Sr, Cd, and Bi); an initial calibration blank of deionized H_2O; used etchant solution; blank sample; sample reagent blank solution; blank sample; the calibration validation standard; and a calibration blank of deionized H_2O. All measurements were made during a single analytical session and the estimated elemental concentrations were determined with an estimated uncertainty of 20% (based on instrument specifications).

3. Results and discussion

The analysis of crystal performance as radiation spectrometers prior to E-etching is shown in Fig. 1 for an ^{241}Am source (FWHM in keV of 13.62 (D2) and 14.4 (E3)). Analysis with a ^{57}Co source yielded FWHM values in keV of 13.73 and 14.12 for D2 and E3, respectively (data not shown). A plot of the centroid of the ^{137}Cs source (300 V bias, 0.5 μs shaping time) as a function of electric field (E) was also measured. The $\mu\tau_e$ values of 1.1×10^{-3} cm^2/V for D2 and 0.9×10^{-3} cm^2/V for E3[1] were subsequently calculated from this plot using the modified Hecht relationship as follows:

$$\frac{Q}{Q_0}=\lambda_e D^{-1}(1\text{-}e^{-(D/\lambda e)})$$

where Q is the charge collected, Q_0 the nominal charge generated by the incident radiation, D the device thickness, x the depth of interaction from the cathode, λ the carrier drift length (electrons in this case), which is the product of the carrier mobility (μ), lifetime (τ), and the electric field E [20–23].

Performance data, along with $\mu\tau_e$ measurements indicate that both the crystals are good performers as room-temperature gamma-ray spectrometers.

AFM and optical data reveal that prior to E-etching, the CZT surface is highly scratched (Fig. 2) due to the mechanical polishing steps. While optical images suggest a relatively smooth surface with a very low number of surface defects, AFM images of D2 (Fig. 2b) reveal that some mechanical damage still exists on the

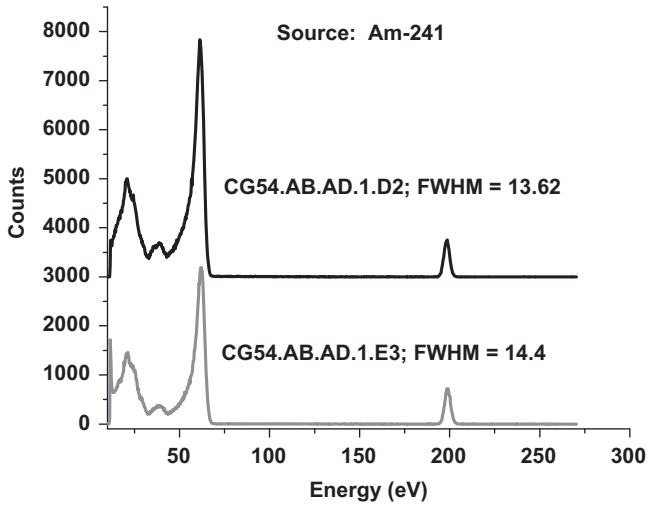

Fig. 1. Radiation spectrometer data for both crystals using an ^{241}Am source (200 V bias, electric field = 1058.2 V/cm). Tennelec amplifier settings were as follows: 1 K coarse gain; 0.25 μs × 2 μs; and 10.62 fine gain. The peaks observed at ~198 eV are the Pulser peaks to measure the electronic noise.

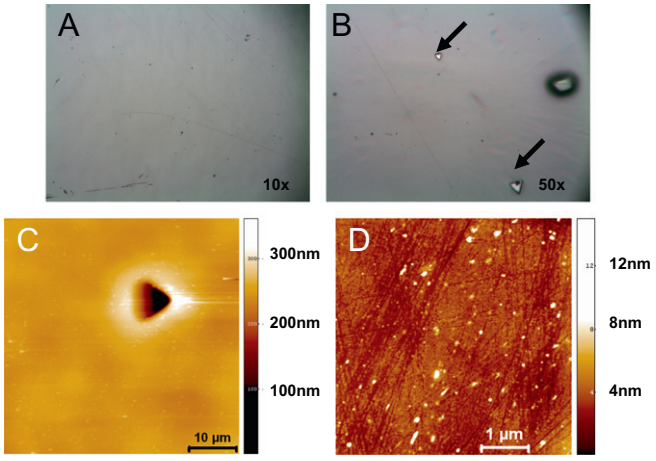

Fig. 2. Optical and AFM images of CZT surface (crystal D2) before exposure to Everson etch. Optical image in (A) taken at 10× magnification and optical image in (B) taken at 50× magnification show some scratches on the surface. Arrows indicate additional triangular features observed in (B), which are most likely surface terminated SPs. The AFM image in (A) shows a surface terminated void SP (scale bar = 10 μm), while the higher-resolution AFM image in (B) shows that surface damage (scratches) from mechanical polishing still exist following Br-MeOH treatment, prior to Everson etching (scale bar = 1 μm).

[1] We note that the $\mu\tau_e$ values will be ~2–2.5 times higher if the shaping time is changed to 3 μs.

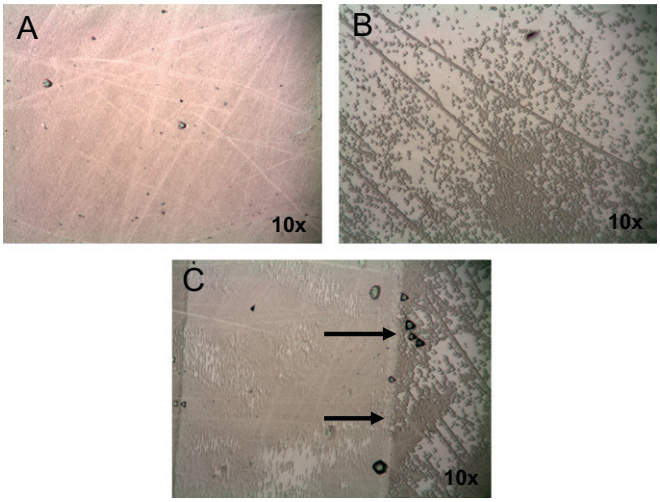

Fig. 3. Optical images of CZT surface (D2) after exposure to Everson etch. Seemingly low (A) and high (B) etch pit densities observed, with some etch pits oriented in lines across the surface (B). Arrows indicate the different crystal orientations exposed (C).

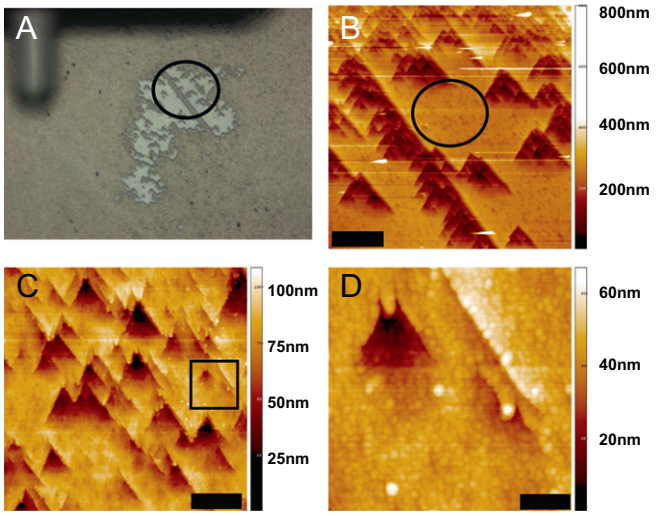

Fig. 4. Non-contact mode AFM images of CZT surface (D2) after exposure to E-etchant. (A) Optical image taken in AFM. Circle indicates approximate location of area scanned by AFM and shows etch pits oriented in a line. (B) 49 μm × 49 μm AFM image of area shown in (A) in which some of the EPs are oriented along a line (scale bar=10 μm). (C) 5 μm × 5 μm AFM image of area circled in (B) showing further pitting of the surface in regions that are seemingly smooth in optical images (scale bar=1 μm). (D) High-resolution AFM image of square area shown in (C), which shows EPs approximately 200–250 nm in width (scale bar=200 nm).

surface following exposure to the Br-MeOH etch. Similar mechanical damage is also observed in AFM images of the surface of E3 which was not exposed to a Br-MeOH etch.

Optical images reveal a variety of different features ranging from larger, triangular pits/mounds similar to those reported in previous etching studies [13–17] to different crystal orientations (Fig. 3(c)). On initial inspection, some regions (Fig. 3(a)) suggest a low EP density (EPD), while others (Fig. 3(b)) reveal EPs oriented in lines along the surface. AFM provides a nanoscale view of the surface structure and reveals EPs on the surface ranging in size from ~200 nm to 10 μm. This method is comparable to previous chemical etching studies on CZT and CdTe using optical and SEM methods that report EPs ranging in size from ~2 to 20 μm and previous etching studies on CdTe/Si epilayers using SEM and AFM that report EPs ranging in size from ~1–3 μm [13–17, 19].

AFM images (Figs. 4 and 5) of different surface regions also reveal that significant etching occurs over the entire surface, even in areas that, from optical images, appear to be smooth. We note that the additional Br-MeOH etch on crystal D2 did not appear to have a large impact on the types of surface features observed following exposure to the E-etch. This is most likely attributed to the fact that the Br-MeOH etch (as applied here) did not completely remove the mechanical polishing surface damage.

One of the most interesting observations from our studies is the presence of EPs on the order of a few hundred nanometers on the CZT surface, even in areas that are seemingly smooth under optical microscopy. We also find, in several areas, a linear alignment of EPs ranging in size from ~5 to 10 μm. This type of linear alignment of EPs has been previously attributed to the presence of dislocation lines in the crystal [14]. While some evidence of this alignment is suggested by the AFM and optical data shown in Fig. 5, the data in Figs. 3 and 4 challenge the aforementioned general conclusions from previous studies that attribute EP alignment to dislocation lines.

During mechanical polishing, scratching exposes new surface area. This polishing process is likely to weaken bonds and present surface sites that are reactive to the various components of the etchants. Given that our results show a large EPD ranging from the nm to the μm scale, we find that the pre-etching surface treatments greatly influence the number of active surface sites and the resultant surface EPD.

We performed ICP-MS analysis on the used etchant solution to determine the amount and ratio of Cd, Zn, and Te that is released upon etching (as shown in Table 1). The results indicate that an increased amount of Cd, Zn, and Te exists in the used etchant sample compared to that of the reagent blank sample that was not exposed to the crystal. It is also noted that there is an excess of Cd present in the used etchant compared to that of Te (Cd:Zn:Te in the used etchant is ~2.1:0.1:1). As this ratio is not equal to that of the bulk ($Cd_{(1-x)}Zn_{(x)}Te$), one might initially conclude that, in

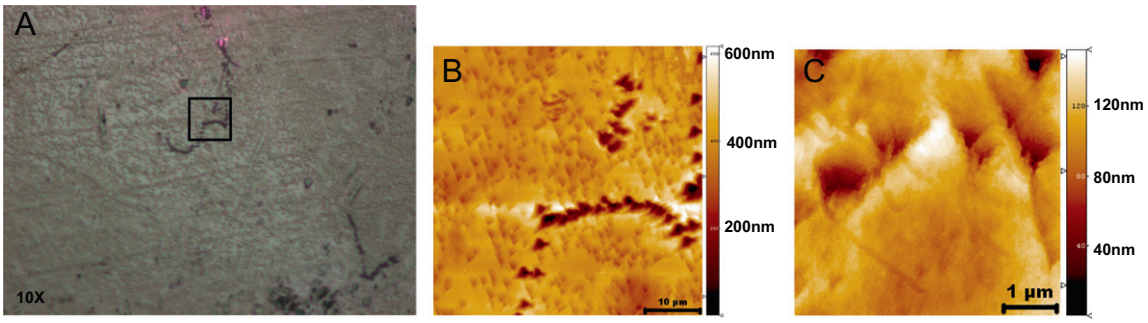

Fig. 5. Optical and non-contact mode AFM images of CZT surface (E3) after exposure to E-etchant. (A) Optical image taken in AFM. Square indicates approximate location of area scanned by AFM and shows EPs oriented in a curved line, similar to previous etching studies in which EPs are located at dislocation lines [14]. (B) AFM image of area indicated in (A) showing zoom in EPs oriented in a curved line (scale bar=10 μm). (C) Zoom in of area in (B) (scale bar=1 μm).

Table 1
Concentrations are listed (in ppb) of elements in standard, blank, and sample solutions as determined by ICP-MS.

Element	NIST traceable standard concentration (ppb)	Initial calibration validation standard (ppb)	Initial calibration blank (ppb)	Used etchant sample (ppb)	Reagent blank sample (ppb)
Li	50	22	0.021	0.047	0.17
Mg	50	22	0.37	25	170
Co	50	24	0.012	0.63	0.46
Ni	50	22	0.048	10	16
Zn		0.31	0.082	1300	94
Sr	50	22	0.021	0.91	1.1
Cd	50	22	<0.026	23,000	4.1
In	10	10	10	10	10
Te		<0.085	<0.092	11,000	2.1
Bi	50	24	0.015	0.98	0.44

contrast to previous studies [14], the E-etchant preferentially attacks the Cd in the bulk crystal.

The location of EPs from N- and E-etchings have been attributed to the areas where surface exit points are associated with crystalline defects. In CZT, those defects that are known to occur as small volume, heterogeneous phases that can exist as filled, partially filled and void SPs within the bulk phase [5,9]. Historically, these SPs have been described with the following terms: precipitates, inclusions, impurities, decorations at grain boundaries, decorations at twin boundaries, and pipes. Other defects that have been observed include changes in crystal orientation due to twinning and grain boundaries. These differences in crystal orientation may coincide with the existence of other SPs as in the usage of the terms "decorations at grain boundaries". The SP can also be found in a dispersed or cellular arrangement. But in general, defects such as those previously described are often associated with material that has high leakage currents, poor charge collection, and excessive charge trapping as previously noted [4,24].

These defects in CZT can present locations for surface-controlled interactions that are exposed by etchants. Due to their different activation energies, surface sites that contain kinks, ledges, steps, and adatoms are likely to present a variety of areas for surface reactions. Those areas with SP voids, partially filled voids and Te oxide are also potentially reactive. This may be due to their physical shape, but it may well be due to their oxidation state composition [e.g., Te(+IV) oxide vs. metallic CdZnTe metal].

Although ICP-MS analysis of the used etchant shows an increased concentration of Cd with respect to that of Zn and Te, we conclude that this most likely results from the nature of the etching solution itself and the ability of the Cd and Zn (in the bulk of the crystal) to complex with the various ions in solution compared to the that of Te (in the bulk of the crystal), which may not readily complex with the etching solution given its negative oxidation state in the bulk of the crystal compared to that of Te in defects as discussed previously. In our case, the etchant solution is largely lactic acid with small amounts of HF and HNO_3. These stronger acids (HF and HNO_3) will attack the CdZnTe crystal, forming largely Cd(+II) and Te(−II) ions in solution. The Te(−II) anions may react with H^+ forming gaseous H_2Te that is liberated from the etchant solution. The NO_3^- anion is also a sufficiently vigorous oxidizing agent that may convert some of the Te(−II) to Te(0) (metal), which is not water soluble and may also be colloidal, which is insoluble. It is likely that some of this Te metal is redeposited on the crystal surface, and may potentially be responsible for the black layer that is observed in our studies and previous etching studies of CdZnTe following exposure to these types of etchants (containing strong acids such as HF). In contrast, the Cd(+II) and Zn(+II) cations both form strong complexes with lactate and nitrate and would be soluble in the etching solution. Given this chemistry, we can expect some loss of Te species in our used etchant solution prior to ICP-MS analysis. In general, our initial mass spectrometry results do not suggest preferential attack of Te species commonly associated with crystalline defects.

We also gain insight into the etching process by comparing the detector performance measurements with optical and AFM images of the etched surface. If the EP density observed in optical and AFM images is proportional to the density of defects, dislocations, and Te precipitates, one would expect that this crystal would have a much lower performance as a radiation spectrometer. From optical images, similar to those shown in Fig. 3(b) that reveal larger EPs on the μm scale, we estimate an EPD of $\sim 7.6\times10^{-3}\,\mu m^{-2}$. However, the number of smaller EPs observed in our AFM studies (those not resolved by optical microscopy), clearly demonstrate that the EPD is much larger than this estimate. Furthermore, we observe linear alignment of EPs on the surface, the majority of which is most likely associated with surface damage caused by mechanical polishing.

We recognize that previous studies on these types of "pitting" etchants (the N-etch and E-etch) report etching and polishing procedures that are inconsistent. While most groups employ a series of mechanical polishing steps prior to etching, other pre- or post-etching treatments may also be employed. These may be in the form of the Br-MeOH pre-etch as reported here for sample D2 or a post-etch with Br-MeOH following pitting of the surface [14]. Regardless, the length and concentration of exposure to these pre-etching chemical treatments will also influence the chemical composition of the surface terminating layer as well as influencing the surface roughness (number and variety of surface sites).

4. Conclusions

We have shown high-resolution AFM images of the CZT surface before and after using the E-etch method. Our results reveal that although this etching method has the potential to be used to examine crystal quality and for assessing dislocation density and distribution, the relationships between the exposed EPs, the dislocation density of the crystal, and the performance of the crystal as a radiation spectrometer will require a closer examination. From the data shown here, we can conclude that: (1) EPD is strongly influenced by the pre-etching surface preparation methods (both mechanical and chemical treatment) and (2) estimations of EPD from optical methods do not measure the number of nanoscale EPs formed on the surface that may also result from defects near the crystal surface. Due to the general

nature of surface dissolution reactions, which are typically transport or surface controlled (or a combination thereof), our conclusions reveal that mechanical polishing, is responsible for the high EPD observed. Etchants that are acidic and have ligands (such as lactate and F^-, as with the E-etch) should be more reactive toward larger number of surface sites than those that are only acidic like the Br-MeOH etch and we find it unreasonable to assume that all defects will be made visible through etching or that all etchants will behave similarly with CZT.

Acknowledgements

This document was prepared in conjunction with work accomplished under Contract no. DE-AC09-08SR22470 with the U.S. Department of Energy. This work was supported by US DOE—National Nuclear Security Administration, through the Office of Nonproliferation and Verification Research and Development—NA-22 Grant no. DE-FG52-05NA27035. R.S. and K.G.L. would like to thank the services of Dr. Kelly Alan Jones and Mr. Santosh Swain from the Center for Materials Research, Washington State University, Pullman, WA, for their help with the growth of CG54.

Disclaimer

References

[1] A.E. Bolotnikov, G.S. Camarda, G.A. Carini, Y. Cui, L. Li, R.B. James, Nucl. Instr. and Meth. A 571 (2007) 687.
[2] A. Burger, K. Chattopadhyay, H. Chen, X. Ma, J.O. Ndap, M. Schieber, T.E. Schlesinger, H.W. Yao, J. Erickson, R.B. James, Nucl. Instr. and Meth. A 448 (2000) 586.
[3] J.F. Butler, C. Lingren, F.P. Doty, IEEE Trans. Nucl. Sci. NS-6 (1992) 605.
[4] G.A. Carini, A.E. Bolotnikov, G.S. Camarda, G.W. Wright, R.B. James, L. Li, Appl. Phys. Lett. 88 (2006) 143515.
[5] M.C. Duff, D.B. Hunter, A. Burger, M. Groza, J.P. Bradley, G. Giles, Z. Dai, D.R. Black, H. Burdette, A. Lanzirotti, J. Mater. Res. 24 (2009) 1361.
[6] M.C. Duff, D.B. Hunter, A. Burger, M. Groza, V. Buliga, D.R. Black, Appl. Surf. Sci. 254 (2008) 2889.
[7] J.R. Heffelfinger, D.L. Medlin, R.B. James, MRS Symp. Ser. 487 (1998) 33.
[8] M. Schieber, T.E. Schlesinger, R.B. James, H. Hermon, H. Yoon, M. Goorsky, J. Cryst. Growth 237–239 (2002) 2082.
[9] T.E. Schlesinger, J.E. Toney, H. Yoon, E.Y. Lee, B.A. Burnett, L. Franks, R.B. James, Mater. Sci. Eng. R 32 (2001) 103.
[10] J. Shen, D.K. Aidun, L. Regel, W.R. Wilcox, J. Cryst. Growth 132 (1993) 250.
[11] C. Szeles, M.C. Driver, SPIE 3446 (1998) 1.
[12] T. Wang, W.Q. Jie, D.M. Zeng, Mater. Sci. Eng. A 472 (2008) 227.
[13] W.J. Everson, C.K. Ard, J.L. Sepich, B.E. Dean, G.T. Neugebauer, J. Electron. Mater. 24 (1995) 505.
[14] A. Hossain, A.E. Bolotnikov, G.S. Camarda, Y. Cui, G. Yang, R.B. James, J. Cryst. Growth 310 (2008) 4493.
[15] Y. Jianrong, G. Huiming, C. Xinqiang, F. Weizheng, H. Li, J. Cryst. Growth 234 (2002) 337.
[16] E. Saucedo, P. Rudolph, E. Dieguez, J. Cryst. Growth 310 (2008) 2067.
[17] J. Shen, D.K. Aidun, L.L. Regel, W.R. Wilcox, J. Cryst. Growth 132 (1993) 351.
[18] K. Nakagawa, K. Maeda, S. Takeuchi, Appl. Phys. Lett. 34 (1979) 574.
[19] J.D. Benson, et al., J. Electron. Mater. 38 (2009) 1771.
[20] C.J. Johnson, E.E. Eissler, S.E. Cameron, Y. Kong, S. Fan, S. Jovanovic, K.G. Lynn, Mat. Res. Soc. Symp. Proc. 302 (1993) 463.
[21] K. Hecht, Z. Phys. 77 (1932) 235.
[22] K.A. Jones, A. Datta, K.G. Lynn, L.A. Franks, J. Appl. Phys. 107 (2010) 123714.
[23] D.S. McGregor, Z. He, H.A. Seifert, R.A. Rojeski, D.K. Wehe, IEEE Trans. Nucl. Sci. NS-45 (1998) 443.
[24] C. Szeles, W.C. Chalmers, S.C. Cameron, J.O. Ndap, M. Bliss, K.G. Lynn, SPIE 4508 (2001) 57.